ELSEVIER

1 October 1999

Optics Communications 169 (1999) 357–367

OPTICS COMMUNICATIONS

www.elsevier.com/locate/optcom

Full length article

Multimode instabilities in the transit-multistable ring cavity

A.T. Rosenberger [a,*], J.P. Rezac [a], Jeong-Mee Kim [b]

[a] *Department of Physics and Center for Laser and Photonics Research, Oklahoma State University, Stillwater, OK 74078-3072, USA*
[b] *Optical Communications R&D Group, Samsung Electronics, Suwon 440-600, South Korea*

Received 25 June 1999; accepted 29 July 1999

Abstract

The transmission of a ring resonator, whose nonlinear medium is a beam of resonant two-level atoms with transit time shorter than their spontaneous lifetime, exhibits multistability. The stability of multiple longitudinal modes in such a system is analyzed for cavities tuned both to resonance and midway between resonances, with atoms injected in an eigenstate or in superposition states. Regions of instability are identified and are usually found to be locally associated with the multiple segments of the transmission function (state equation) that have negative slope. However, in some cases, the transmission is found to be globally unstable; the instability region covers a large continuous range of input field. This is because, in contrast to the usual multimode instability, the imaginary part of the field contributes even when atoms and cavity are both resonant with the driving laser.

PACS: 42.65.Sf; 42.65.Pc; 42.50.Gy
Keywords: Multistability; Multimode instability; Mesomaser; Transit effects; Coherent injection

1. Introduction

When an optical ring resonator contains a medium consisting of a monoenergetic beam of two-state atoms, and the transit time of these atoms through the cavity mode is smaller than their spontaneous lifetime, light transmitted through the nonlinear resonator can show multistability [1,2]. This is a result of the atoms' Rabi cycling in transit, and is essentially identical to the behavior found in the mesomaser [3–6]. Consider atoms injected in their ground state and neglect spontaneous emission; atoms passing through the cavity mode will experience an effective pulse. If this pulse has area $(2n+1)\pi$, where n is an integer, the atoms will carry energy out of the resonator, thereby reducing the optical transmission. However, atoms seeing a $2n\pi$ pulse return all absorbed energy to the resonator mode via stimulated emission, and in this case the transmission is that of an empty resonator. Since the effective pulse area depends on the intracavity field, the result is an input–output curve that can show bistability, multiple regions of bistability, or multistability, depending on the density of the atomic beam and the finesse of the resonator.

The multistability would be severely degraded by using a beam with a large spread of atomic speeds, but a velocity-selected beam with a relative velocity spread of 10% gives essentially the same results as a monoenergetic beam [1,3], so the beam will be assumed monoenergetic here. Spontaneous emission also degrades the multistability [1,2], so we will take

* Corresponding author. E-mail: atr@okstate.edu

0030-4018/99/$ - see front matter
PII: S0030-4018(99)00424-1

the atomic transit time to be much shorter than the spontaneous lifetime. Likewise, a Gaussian transverse dependence of the resonator mode somewhat reduces the multistable behavior [1,2]; for simplicity, in this study we will treat the mode as a hard-edged plane wave, so that an atom passing through sees an effective square pulse. The atomic medium is therefore homogeneously broadened due to the finite transit time.

The steady state, single-mode stability properties, and related dynamical behavior have been studied for such transit-multistable systems for the cases of atoms injected in either the ground [1–5] or the excited [3,6] state. The latter case is essentially the same problem as that of the monovelocity beam maser [7–9]. All of this semiclassical analysis [1–9] applies not only to macroscopic systems, but also down to the mesoscopic scale, where the number of atoms in the resonator is perhaps a few hundred; it is, however, inappropriate for few-atom systems such as the micromaser.

In this work, we consider the steady-state behavior and multimode stability of the nonlinear resonator with atoms injected not only in the ground and excited energy eigenstates, but also in coherent superpositions of the two eigenstates, specifically those produced by the interaction of ground-state atoms with an effective $\pi/2$ or $3\pi/2$ pulse by passing through a resonant preparation beam just before entering the resonator mode. (Steady-state response of the micromaser with similar coherent injection was studied in Refs. [10–12].) These superpositions have equal probabilities for finding the atoms in either eigenstate, but the resonator transmission is very different from the effectively empty-cavity transmission that would result from the injection of equal numbers of ground-state and excited-state atoms. For all injected states, multistability is found and the regions of instability are identified; those regions show a qualitative dependence on the state of the injected atoms. Even when both the atoms and the cavity are resonant with the driving laser, the imaginary part of the field contributes to the instability. This stands in strong contrast to the usual case of multimode instabilities with homogeneously broadened, but non-transiting, atoms (''stationary'' atoms).

In the analysis that follows, the atoms are assumed to be resonant with the incident light in all cases. The model, including the steady-state solutions for a resonant cavity, is presented in Section 2. The linear stability analysis of this resonant-cavity model is the subject of Section 3. The model for a cavity driven midway between longitudinal modes is given in Section 4, along with an extension of the stability analysis to the multimode case. Section 5 contains a discussion of our results, and conclusions are given in Section 6.

2. Model and steady-state response

Although our earlier theoretical approach [1,2] is fully equivalent to that of Refs. [3–6], we will adopt the latter approach here because it lends itself more readily to stability analysis. The evolution of the system is described by the following Maxwell–Bloch equations for both atoms and cavity resonant with the field:

$$\left(\frac{\partial}{\partial t}+\frac{\partial}{\partial T}\right)v(T,t)=\frac{x_r(t)}{\tau}w(T,t), \tag{1}$$

$$\left(\frac{\partial}{\partial t}+\frac{\partial}{\partial T}\right)u(T,t)=\frac{x_i(t)}{\tau}w(T,t), \tag{2}$$

$$\left(\frac{\partial}{\partial t}+\frac{\partial}{\partial T}\right)w(T,t)=-\frac{x_r(t)}{\tau}v(T,t) - \frac{x_i(t)}{\tau}u(T,t), \tag{3}$$

$$\frac{\mathrm{d}x_r(t)}{\mathrm{d}t}=-k\left[x_r(t)-y-\frac{4C}{\tau}\int_0^{\tau}v(T,t)\mathrm{d}T\right], \tag{4}$$

$$\frac{\mathrm{d}x_i(t)}{\mathrm{d}t}=-k\left[x_i(t)-\frac{4C}{\tau}\int_0^{\tau}u(T,t)\mathrm{d}T\right]. \tag{5}$$

Eqs. (1)–(3) describe the behavior of the atoms, and Eqs. (4) and (5) that of the cavity field. The Bloch vector transverse components v and u are proportional to the real and imaginary parts of the atomic polarization, and the longitudinal component of the Bloch vector, w, is proportional to the population inversion. The dimensionless intracavity field is denoted by $x=x_r+ix_i=\Omega\tau$, where Ω is the complex intracavity Rabi frequency and τ is the transit

time. Eqs. (1)–(3) include no spontaneous decay terms because $\tau \ll \tau_{sp}$ (where τ_{sp} is the spontaneous lifetime); thus the state of an atom is changed only by interaction with the cavity field, which can vary in time, as shown in Eqs. (4) and (5). The state of an atom will vary with position as the atom passes through the mode, even if the cavity field is constant (steady state), and this is represented by the T-dependence of u, v and w. An atom located a distance z into the mode has been in the mode for a time $T = z/v_a$, where v_a is its speed; T satisfies $0 \le T \le \tau$. The cavity field decay rate is given by k. The dimensionless incident field, y, taken to be real, is the product of the transit time and the (real) value that the steady-state intracavity Rabi frequency would take in the absence of atoms; note that just as y and x give the intracavity field of the empty and filled cavities when multiplied by the same constant, they also give the incident and transmitted fields when multiplied by another constant. The cooperativity C is, as usual, one-half the ratio of the atomic loss to the resonator loss; however, in this system, the dominant atomic loss is escape from the resonator mode, determined by the transit time rather than the spontaneous lifetime. This means that $C = C_{st}\tau/4\tau_{sp}$, where C_{st} is the usual cooperativity value for the same number of stationary atoms interacting with the cavity mode.

In steady state, Eqs. (1)–(5) become

$$\frac{\mathrm{d}}{\mathrm{d}T} v(T) = \Omega w(T), \tag{6}$$

$$\frac{\mathrm{d}}{\mathrm{d}T} w(T) = -\Omega v(T), \tag{7}$$

$$y = x - \frac{4C}{\tau}\int_0^{\tau} v(T)\mathrm{d}T, \tag{8}$$

where x (thus Ω) is taken to be real, and u to be zero, without loss of generality. Eq. (8) is the input–output relation, or state equation.

The form taken by the state equation is determined by the state of the atoms as they enter the cavity mode. Atoms prepared in an eigenstate have $v(0) = 0$ and $w(0) = \mp 1$, where the upper sign is for injection of ground-state atoms (prepared by a 0π pulse) and the lower sign for injection of excited-state atoms (prepared by a π pulse). Thus

$$v(T) = \mp \sin(\Omega T), \tag{9}$$

$$w(T) = \mp \cos(\Omega T), \tag{10}$$

and

$$y = x \pm 4C\frac{1-\cos x}{x}. \tag{11}$$

Atoms injected in the two superposition states considered here have $w(0) = 0$ and $v(0) = \mp 1$, being prepared by $\pi/2$ (upper sign) or $3\pi/2$ (lower sign) pulses, giving

$$v(T) = \mp \cos(\Omega T), \tag{12}$$

$$w(T) = \pm \sin(\Omega T), \tag{13}$$

and

$$y = x \pm 4C\frac{\sin x}{x}. \tag{14}$$

The steady-state multistable transmission represented by Eq. (11) has been analyzed in Refs. [1–6]. Similar multistability is exhibited by Eq. (14), and both cases are discussed further in Section 5.

3. Linear stability analysis

We now consider Eqs. (1)–(5), and linearize about the steady-state solutions $v(T)$, $w(T)$ and x (with $u = 0$ and $x_i = 0$), that were found above. We take y to be real, but must allow the perturbed x to be complex. With the usual *ansatz*, namely that the time dependence of the perturbations is exponential with a complex eigenvalue λ, we have:

$$v(T,t) = v(T) + \delta v(T,t) = v(T) + \delta v(T)e^{\lambda t}, \tag{15}$$

$$u(T,t) = \delta u(T,t) = \delta u(T)e^{\lambda t}, \tag{16}$$

$$w(T,t) = w(T) + \delta w(T,t) = w(T) + \delta w(T)e^{\lambda t}, \tag{17}$$

$$x_r(t) = x + \delta x_r(t) = x + \delta x_r e^{\lambda t}, \tag{18}$$

$$x_i(t) = \delta x_i(t) = \delta x_i e^{\lambda t}. \tag{19}$$

The linearized Eqs. (1)–(5) for the perturbations are then written as follows:

$$\left(\lambda + \frac{\mathrm{d}}{\mathrm{d}T}\right)\delta v(T) - \frac{1}{\tau}\left[\delta x_r w(T) + x\delta w(T)\right] = 0, \tag{20}$$

$$\left(\lambda + \frac{\mathrm{d}}{\mathrm{d}T}\right)\delta u(T) - \frac{1}{\tau}\delta x_i w(T) = 0, \tag{21}$$

$$\left(\lambda + \frac{\mathrm{d}}{\mathrm{d}T}\right)\delta w(T) - \frac{1}{\tau}\left[\delta x_r v(T) + x\delta v(T)\right] = 0, \tag{22}$$

$$(\lambda + k)\delta x_r - \frac{4Ck}{\tau}\int_0^\tau \delta v(T)\mathrm{d}T = 0, \tag{23}$$

$$(\lambda + k)\delta x_i - \frac{4Ck}{\tau}\int_0^\tau \delta u(T)\mathrm{d}T = 0. \tag{24}$$

In Eqs. (20)–(24), the initial (at injection) Bloch vector perturbation is zero, i.e., $\delta v(0) = \delta u(0) = \delta w(0) = 0$. Eqs. (20) and (22) can be combined, using Eq. (6) and the relation $x = \Omega\tau$, to give a closed second-order differential equation for δw (the prime indicates a derivative with respect to T),

$$\delta w'' + 2\lambda\delta w' + (\Omega^2 + \lambda^2)\delta w = -\frac{\delta x_r}{\tau}\left[2\Omega w(T) + \lambda v(T)\right], \tag{25}$$

which can easily be solved because the homogeneous solution is a linear combination of $\mathrm{e}^{-\lambda T}\cos(\Omega T)$ and $\mathrm{e}^{-\lambda T}\sin(\Omega T)$, and the right-hand side can be written in the form $A\sin(\Omega T) + B\cos(\Omega T)$, where A and B are determined by the state of the injected atoms, i.e., by Eqs. (9) and (10) or Eqs. (12) and (13). The initial conditions on $\delta w'$ are found from Eq. (22), using Eq. (9) or Eq. (12).

For the case of injection of eigenstate atoms prepared by a pulse of area 0 (ground state, upper sign) or π (excited state, lower sign) we solve Eq. (25) to find

$$\delta w(T) = \pm\frac{\delta x_r}{\lambda\tau}(1 - e^{-\lambda T})\sin(\Omega T). \tag{26}$$

If the injected atoms are prepared in a superposition state by a pulse of area $\pi/2$ (upper sign) or $3\pi/2$ (lower sign), solution of Eq. (25) gives

$$\delta w(T) = \pm\frac{\delta x_r}{\lambda\tau}(1 - e^{-\lambda T})\cos(\Omega T). \tag{27}$$

Now, substituting Eq. (26) into Eqs. (20) and (21) results in, for eigenstate injection,

$$\delta v(T) = \mp\frac{\delta x_r}{\lambda\tau}(1 - e^{-\lambda T})\cos(\Omega T), \tag{28}$$

$$\delta u(T) = \mp\frac{\delta x_i}{\tau(\Omega^2 + \lambda^2)}\left\{\Omega\sin(\Omega T) + \lambda\left[\cos(\Omega T) - e^{-\lambda T}\right]\right\}, \tag{29}$$

or substitution of Eq. (27) into Eqs. (20) and (21) for superposition-state injection gives

$$\delta v(T) = \pm\frac{\delta x_r}{\lambda\tau}(1 - e^{-\lambda T})\sin(\Omega T), \tag{30}$$

$$\delta u(T) = \pm\frac{\delta x_i}{\tau(\Omega^2 + \lambda^2)}\left\{\lambda\sin(\Omega T) - \Omega\left[\cos(\Omega T) - e^{-\lambda T}\right]\right\}. \tag{31}$$

Inserting Eqs. (28) and (29) or Eqs. (30) and (31) into Eqs. (23) and (24) then results in the following equation for the eigenvalue λ (using $x = \Omega\tau$):

$$\lambda = -k\left[1 \mp \frac{4C}{x^2 + \lambda^2\tau^2}J_m(x, \lambda\tau)\right], \tag{32}$$

where association with the real part of the perturbed field (Eq. (23)) is denoted by $m = 1$, and association with the imaginary part of the perturbed field (Eq. (24)) is denoted by $m = 2$. Instability occurs when the eigenvalue λ has a positive real part.

For eigenstate injection, the functions J_m take the form

$$J_1(x, \lambda\tau) = 1 - e^{-\lambda\tau}\cos x - \frac{1}{\lambda\tau}\left(1 - e^{-\lambda\tau} + \frac{\lambda^2\tau^2}{x^2}\right) \times x\sin x, \tag{33}$$

$$J_2(x, \lambda\tau) = \cos x - e^{-\lambda\tau} - \lambda\tau\frac{\sin x}{x}. \tag{34}$$

Eqs. (32)–(34) are exactly the conditions first found in Ref. [3].

Superposition state injection leads to the following forms for J_m:

$$J_1(x,\lambda\tau) = \frac{\lambda\tau}{x} + e^{-\lambda\tau}\sin x - \frac{1}{\lambda\tau}\left(1 - e^{-\lambda\tau} + \frac{\lambda^2\tau^2}{x^2}\right) x\cos x, \tag{35}$$

$$J_2(x,\lambda\tau) = \frac{x^2+\lambda^2\tau^2}{x\lambda\tau} - \frac{x}{\lambda\tau}e^{-\lambda\tau} - \frac{\lambda\tau}{x}\cos x - \sin x. \tag{36}$$

Eqs. (35) and (36), together with Eq. (32), represent a new set of conditions that specify the stability of the resonator with atoms injected in superposition states prepared by $\pi/2$ or $3\pi/2$ pumping.

4. Multimode analysis

Multimode instabilities in optically bistable systems have been of theoretical and experimental interest for some time now [13–16]. In the transit-multistable, or mesomaser, system, the single-mode instability has been studied in Refs. [3–6]. In the stability analysis above we have extended the consideration to include the case of injection of atoms in superposition states. We now expand the above analysis to show the multimode character of the instabilities. To do this, we employ a method first used by Carmichael [17] to relate instabilities of the nonlinear cavity driven midway between resonances to the regions of negative slope in the state equation of the cavity driven on resonance. Two major differences between our work and earlier studies of multimode instability will be apparent, both deriving from the fact that our nonlinear medium is a beam of fast atoms. First, we will have multiple regions of negative slope; second, we will have the possibility of J_2-type instability, i.e., instability related to the imaginary part of the field. The fact that the multimode analysis depends on the same functions J_m (Eqs. (33)–(36)) that apply in the single-mode case is another example of the intimate link between single-mode and multimode instabilities in general systems [15].

We assume two of the ring resonator's mirrors to be partially-transmitting, with reflectivity R, assumed to be high $(1-R \ll 1)$; the time for light to make one circuit of the ring is the round-trip time τ_r, and so the cavity field loss rate is given by $k = (1-R)/\tau_r$. For the case of the cavity driven midway between resonances, Eqs. (4) and (5) do not properly describe the evolution of the intracavity field because they are derived assuming a small round-trip change in the field and cannot account for the π round-trip phase accumulated in this case. Nevertheless, the stability analysis presented above also applies to this particular non-resonant cavity case. To show this, we use the cavity boundary conditions to write a map equation giving the real part of the intracavity field, just after passing through the atomic beam and before reaching the exit mirror, in terms of its value one round trip earlier:

$$x + \delta x_r(t+\tau_r) = (1-R)\,y \pm R\left[x + \delta x_r(t)\right] + (1-R)\frac{4C}{\tau}\int_0^\tau \left[\upsilon(T) + \delta\upsilon(T, t+\tau_r)\right] \mathrm{d}T, \tag{37}$$

where the upper sign applies when the driving laser is resonant with a cavity mode, and the lower sign reflects the π round-trip phase accumulated when the driving laser is halfway between modes. For the resonant case, the steady-state solution of Eq. (37) reproduces the state Eq. (8); however, for the mid-mode case, the steady-state solution gives the following state equation:

$$y' \equiv \frac{1-R}{2}y = x - \left[\frac{1-R}{2}\right]\frac{4C}{\tau}\int_0^\tau \upsilon(T)\,\mathrm{d}T \cong x, \tag{38}$$

showing that the transmission depends linearly on the input, because the atomic loss is now negligible compared to the cavity loss. In this case, a much larger input field y is needed to produce the same intracavity field x as in the resonant case. (Here, if x is interpreted to be the transmitted field, y is the input field; if x is taken to be the intracavity field with atoms present, y' is the field inside the empty

cavity.) From Eq. (37), the perturbations satisfy the following:

$$e^{\lambda\tau_r}\delta x_r(t) = \pm\left[R\delta x_r(t) + (1-R)\frac{4C}{\tau} \times \int_0^{\tau}\delta v(T,t)\mathrm{d}T\right], \quad (39)$$

where the $\exp(\lambda\tau_r)$ factor that would multiply the small second term on the right-hand side has been replaced by its zeroth-order value, ± 1. Substituting $\pm(1+\lambda\tau_r)$ for the same term on the left-hand side, corresponding to the stability condition being $|\exp(\lambda\tau_r)| < 1$, gives Eq. (23) since the time t is arbitrary and may be taken to be zero. A similar analysis for the imaginary part of the field leads to Eq. (24), showing that Eqs. (23) and (24) apply for mid-mode tuning as well as on cavity resonance. Thus both resonant and mid-mode tuning lead to Eq. (32) for the eigenvalue λ.

In the limit of perfectly reflecting mirrors, the solution of Eq. (39),

$$\exp(\lambda\tau_r) = \pm 1 \Rightarrow \lambda_n^{(0)} = \frac{in\pi}{\tau_r}, \quad (n = 0, \pm 1, \pm 2, \cdots), \quad (40)$$

simply defines the longitudinal modes of the cavity, where n gives the detuning of a given mode from the driving laser in units of half of the cavity's free spectral range. Since the plus sign in Eq. (40) denotes resonance of the laser with a certain mode, the resonant mode is labeled with $n = 0$ and other modes with $n = \pm 2,\ \pm 4$, etc. When the cavity is driven midway between resonances, the modes are labeled with $n = \pm 1,\ \pm 3$, etc. For highly reflecting but not perfect mirrors, the light-atom interaction will result in small perturbation of the eigenvalues in Eq. (40) to

$$\lambda_n = \frac{in\pi}{\tau_r} - k\left[1 \mp \frac{4C}{x^2 + \lambda_n^2\tau^2}J_m(x, \lambda_n\tau)\right], \quad (41)$$

which can be solved to lowest significant order by substituting the unperturbed value of λ_n from Eq. (40) on the right-hand side of Eq. (41). Thus the condition for instability of the mode n, detuned from the driving laser by $n/2$ cavity free spectral ranges, is that the eigenvalue have a positive real part, or:

$$\mathrm{Re}\left[1 \mp \frac{4C}{x^2 - \dfrac{n^2\pi^2\tau^2}{\tau_r^2}}J_m\left(x, \frac{in\pi\tau}{\tau_r}\right)\right] < 0, \quad (42)$$

where again, the upper sign denotes either 0 or $\pi/2$ excitation and the lower sign either π or $3\pi/2$ excitation, using the corresponding functional forms for J_m, Eqs. (35) and (36) for superposition states and Eqs. (33) and (34) for eigenstates. Application of Eq. (42) to the resonant mode $(n = 0)$ gives the instability condition

$$1 \mp \frac{4C}{x^2}J_m(x, 0) < 0, \quad (43)$$

which, upon inspection of the state equations, Eq. (11) and Eq. (14), and using Eqs. (33)–(36) for J_m, reduces, for $m = 1$, in every case of eigenstate or superposition-state injection, to the relation

$$\frac{\mathrm{d}y}{\mathrm{d}x} < 0. \quad (44)$$

For $m = 2$, Eq. (43) leads to

$$\frac{y}{x} < 0, \quad (45)$$

for eigenstate injection, or

$$\frac{y}{x} < \pm\frac{4C}{x}, \quad (46)$$

for superposition-state injection. Thus the resonant mode is unstable (from the real part of the field) in all regions of negative slope of the state equation, and also (from the imaginary part of the field) for all segments of the state equation satisfying the conditions on y/x in Eqs. (45) and (46). We show below how the instabilities of adjacent modes tend to be associated with these resonant-mode instabilities, occurring at approximately the same values of the intracavity field x. For the bistable system with non-transiting atoms, Carmichael [17] showed the association with regions of negative slope, or J_1 instability, as in Eq. (44). We will also see a relation to the J_2 regions, Eqs. (45) and (46).

5. Results and discussion

To illustrate that values of x corresponding to regions of negative slope in the state equation of the driven mode ($n = 0$) also determine the regions of instability both in the resonant cavity (modes of even n) and in the cavity driven midway between resonances (modes of odd n), we will here consider the sidemodes $n = \pm 1$ and $n = \pm 2$ only. For the multistable system, there are many negative-slope regions in the transmission function, as illustrated in Fig. 1 for the case of ground-state atom injection. The state Eq. (11), with the upper sign indicating preparation by a 0π pulse, is plotted in Fig. 1 for $C = 5$. Rabi cycling of the atoms transiting through the field mode in less than a spontaneous lifetime produces multistability (near $y = 13$) in addition to several regions of negative slope. For the state equation of Fig. 1, the regions in the $(\tau/\tau_r) - x$ plane corresponding to instability, as given by Eq. (42), are shown in Fig. 2. Instability may be observed in a positive-slope branch of the resonant-cavity transmission when the even-n unstable regions (dashed lines, for $n = \pm 2$) extend outside the light vertical lines that indicate the negative-slope regions. The regions between the light vertical lines are the J_1-unstable regions of the resonant mode, according to Eq. (44); for ground-state injection the resonant mode has no regions of J_2 instability because the state equation of Fig. 1 never enters the second or fourth quadrants, as required by Eq. (45). Note in Fig. 2 that for certain values of τ/τ_r, the positive-slope branches adjacent to the first negative-slope region become unstable from excitation of the adjacent cavity modes. The J_1 curve (from the real part of the field) extends to the upper positive-slope branch and the J_2 curve (from the imaginary part of the field) extends to both upper and lower branches. For the cavity driven midway between resonances, the state equation will be a straight line of positive slope, as in Eq. (38), and so the entire region within the J_1 and J_2 curves for $n = \pm 1$ (heavy solid lines) represents an observable instability. Note in particular here that both types (J_1 and J_2) of instability are seen for resonant and off-resonant driving, unlike the single-mode instability in the mesomaser [3–6] and multimode instability in the usual stationary-atom bistable system, which show no J_2-type instability.

The horizontal axis in Fig. 2 is the intracavity Rabi frequency (in radians/s) times the transit time, and the vertical axis is the cavity's free spectral range (in Hz) times the transit time. Thus points on a straight line through the origin with slope $(n\pi)^{-1}$ correspond to the Rabi frequency being equal to $n/2$

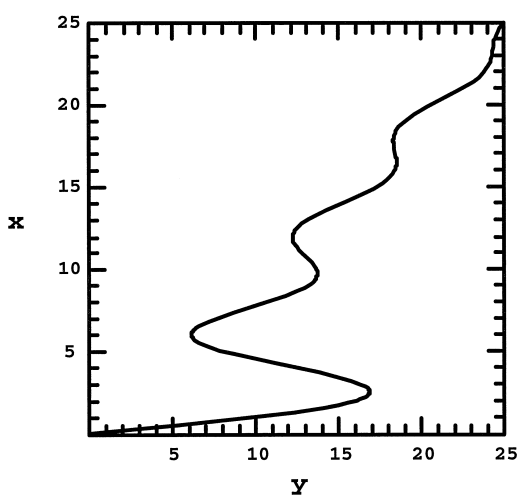

Fig. 1. Output field (x) versus input field (y) for injection of ground-state atoms (0π preparation); $C = 5$.

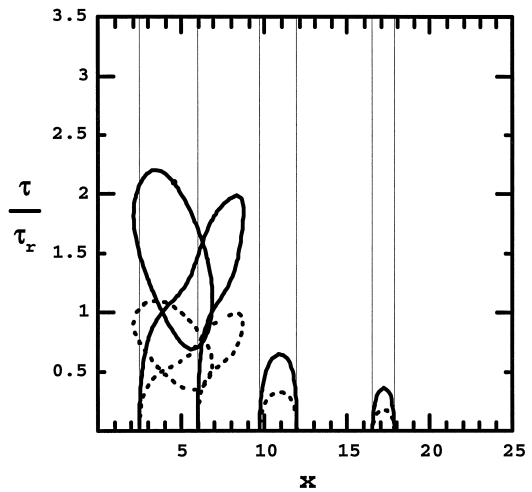

Fig. 2. Instability boundaries for $C = 5$ and 0π preparation, as in Fig. 1. Light lines correspond to $n = 0$; heavy solid and dashed lines indicate $n = \pm 1$ and ± 2, respectively. The x-values between the $n = 0$ lines are the regions of negative slope in Fig. 1. The fingers coming up from the x axis are J_1-type unstable regions, and the closed curves are J_2-type unstable regions.

times the longitudinal mode spacing. These are approximately the slopes of the J_1 fingers in Fig. 2, as would be expected from the weak-sideband-gain interpretation of multimode instability. This interpretation shows that the gain produced in strongly-driven atoms, at a detuning of approximately the Rabi frequency, can lead to instability if a cavity mode is present in the gain region. (See summary in Ref. [15], and references therein.) Consideration of the imaginary part of Eq. (41) will show that mode pulling is not a major concern for the modest values of C of interest here. Therefore we can estimate the fundamental frequency of oscillation of the instability to be equal, for resonant driving, to the cavity's free spectral range, the frequency difference between mode $n = 0$ and modes $n = \pm 2$. In Fig. 2, at $x = 6.75$, the point at $\tau/\tau_r = 0.5$ is on the border of the unstable region; the frequency of oscillation would thus be $2\pi/\tau_r = 3.14/\tau$ (radians/s). In Ref. [3], the frequency of the single-mode instability for $C = 5$ at $x = 6.75$ was found to be $3.06/\tau$. Again, as noted before [15], the close connection between single-mode instability and multimode instability is reflected in the similarity of frequencies, even though the single-mode instability occurs in the bad-cavity limit. Since our instability occurs when τ/τ_r is of order unity, the system is in the good-cavity limit, as expected for multimode instability; the experimental significance of the size of τ/τ_r needed for observation of these various multimode instabilities will be discussed in Section 6.

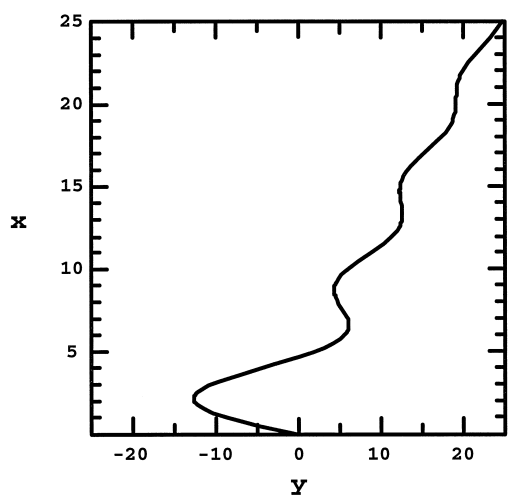

Fig. 3. Output field (x) versus input field (y) for injection of excited-state atoms (π preparation); $C = 5$.

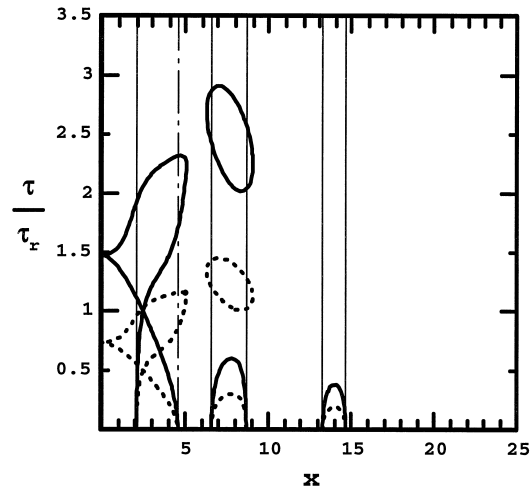

Fig. 4. Instability boundaries for $C = 5$ and π preparation, as in Fig. 3. Light lines correspond to $n = 0$; solid lines for J_1, denoting regions of negative slope in Fig. 3, and dash-dot lines for J_2, corresponding to the second-quadrant part of Fig. 3. Heavy solid and dashed lines indicate $n = \pm 1$ and ± 2, respectively, where the fingers coming up from the x axis are J_1-type unstable regions, and the other curves enclose J_2-type unstable regions.

Fig. 3 shows the state Eq. (11), with the lower sign, for the case of excited-state atomic injection (π-pulse preparation); again, $C = 5$. The fact that the part of the state equation with $y < 0$ is unphysical is reflected in the J_2-type instability region for the resonant mode ($n = 0$) indicated by the light vertical dash-dot line in Fig. 4. Note in Fig. 4 that both the negative-slope and second-quadrant resonant-mode instabilities influence the shapes of the instability boundaries for adjacent modes ($n = \pm 1, \pm 2$). In particular, for mid-mode driving ($n = \pm 1$), the low-x region to the left of the light dash-dot line is accessible because the state Eq. (38) is linear; transmission in this region will be unstable if τ/τ_r is within the heavy solid boundaries.

For injection of atoms prepared by a $\pi/2$ pulse, the state Eq. (14), with upper sign, is shown in Fig. 5; the curve does not start at the origin because the atoms enter the resonator in a superposition state. The corresponding instability boundaries are plotted in Fig. 6, and show several new features. For example, the J_1 fingers reach from the first negative-slope

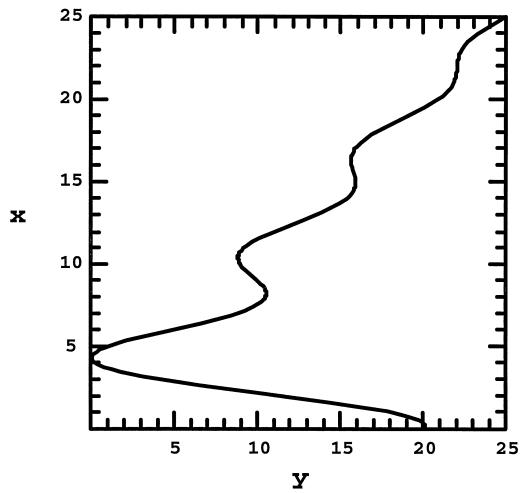

Fig. 5. Output field (x) versus input field (y) for injection of superposition-state atoms prepared by a $\pi/2$ pulse; $C = 5$.

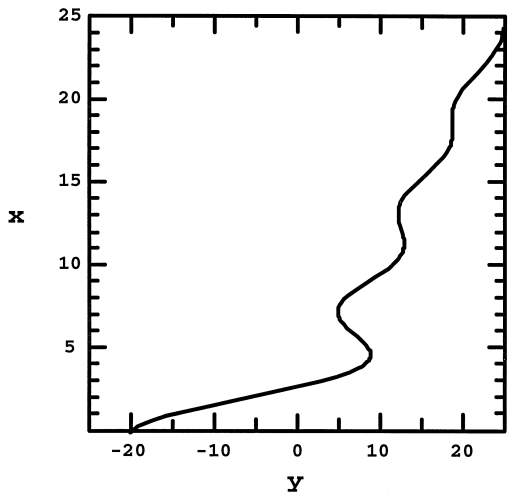

Fig. 7. Output field (x) versus input field (y) for injection of superposition-state atoms prepared by a $3\pi/2$ pulse; $C = 5$.

region into the second. In the resonant cavity ($n = \pm 2$, dashed line), for $\tau/\tau_r \approx 1$, this would make most of the intermediate positive-slope branch unstable, if it weren't already unstable due to J_2 for $n = 0$ (light vertical dash-dot line). In fact, because of the resonant-mode instability condition given in Eq. (46), the entire transmission curve of Fig. 5 is unstable for $y < 4C$. We believe this to be the first time that such an instability has been predicted. Related to this, for the non-resonant cavity ($n = \pm 1$, dashed lines), in contrast to the cases of atoms injected in the ground or excited state, the extent of the J_2 region for small

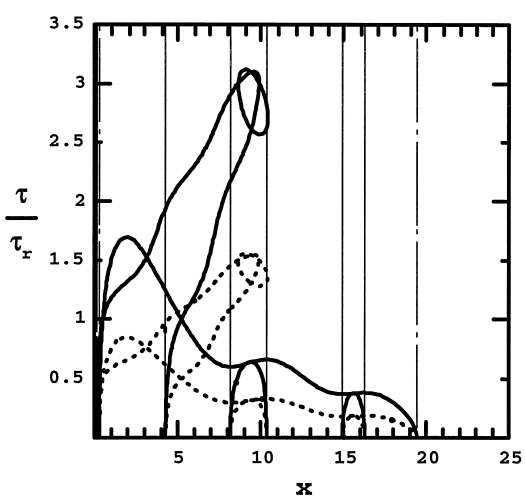

Fig. 6. Instability boundaries for $C = 5$ and $\pi/2$ preparation, as in Fig. 5. Light lines correspond to $n = 0$; solid lines for J_1, denoting regions of negative slope in Fig. 5, and dash-dot lines for J_2, where $y < 4C$. Heavy solid and dashed lines indicate $n = \pm 1$ and ± 2, respectively, where the fingers coming up from the x axis are J_1-type unstable regions, and the other curves enclose J_2-type unstable regions.

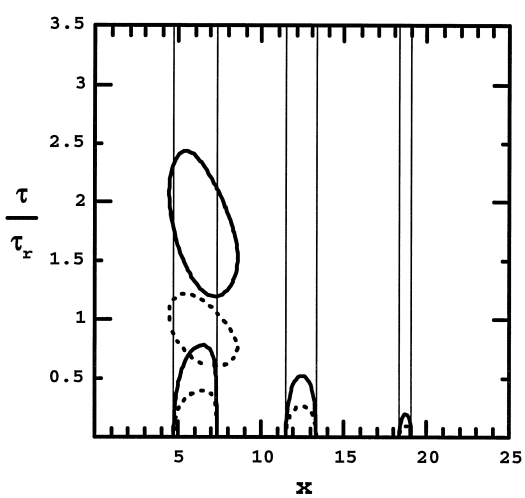

Fig. 8. Instability boundaries for $C = 5$ and $3\pi/2$ preparation, as in Fig. 7. Light solid lines correspond to $n = 0$ and denote regions of negative slope in Fig. 7. Heavy solid and dashed lines indicate $n = \pm 1$ and ± 2, respectively, where the fingers coming up from the x axis are J_1-type unstable regions, and the closed curves are J_2-type unstable regions.

τ/τ_r makes the output unstable at all values of intracavity field within a range that encompasses all regions of negative slope in the resonant state equation as well as the regions between them, covering the entire $y < 4C$ region as τ/τ_r goes to zero.

The results of Figs. 5 and 6 are qualitatively different from the behavior observed in any other case, as Figs. 7 and 8 show for injection of $3\pi/2$-pulse prepared atoms. Fig. 7 is a plot of Eq. (14), using the lower sign. Unlike the $\pi/2$ case of Fig. 6, Fig. 8 shows no J_2-type instability region for $n = 0$ because y is always greater than $-4C$; thus there is no continuous instability region for other modes. Some J_2 regions of instability here do, however, extend beyond the negative-slope parts of Fig. 7, as seen before in Figs. 2 and 4.

In Figs. 9 and 10, the case of $\pi/2$-pulse preparation is shown for an atomic beam with three times the density so that $C = 15$. Here, there are many more regions of negative slope — not only multiple regions of bistability are evident in Fig. 9, but also one region of tristability, around $y = 16$. The instability boundaries are likewise more complex, but again show the global J_2-type instability for the resonant mode and the corresponding global instability for the mid-mode-driven cavity for small τ/τ_r. Note that the J_1 fingers from the lowest-x region extend over many hysteresis loops of the resonant state equation, and that the ends of the fingers from the next lower region have pinched off and appear as closed curves. For increasing C, the instability boundaries continue to increase in complexity.

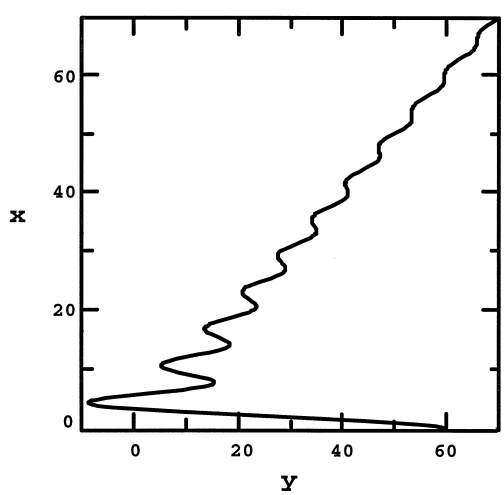

Fig. 9. Output field (x) versus input field (y) for injection of superposition-state atoms prepared by a $\pi/2$ pulse; $C = 15$.

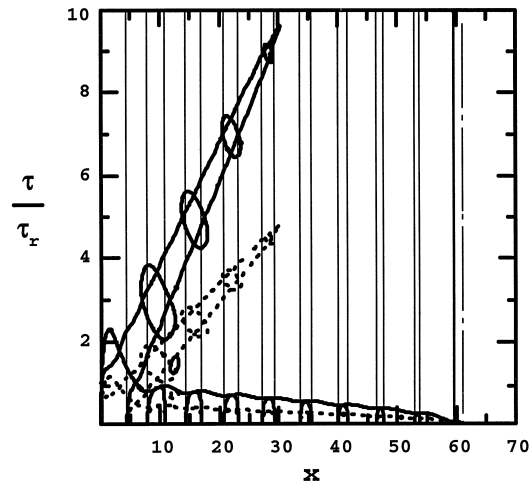

Fig. 10. Instability boundaries for $C = 15$ and $\pi/2$ preparation, as in Fig. 9. Light lines correspond to $n = 0$; solid lines for J_1, denoting regions of negative slope in Fig. 9, and dash-dot lines for J_2, where $y < 4C$. Heavy solid and dashed lines indicate $n = \pm 1$ and ± 2, respectively, where the fingers coming up from the x axis are J_1-type unstable regions, and the other curves enclose J_2-type unstable regions, except those just above $x = 10$, where the ends of the second fingers have pinched off.

6. Conclusions

We have extended the stability analysis of the transit-multistable ring cavity [1,2], sometimes called the mesomaser [3–6], to consider multimode instabilities. Besides considering the cases of atoms injected in their ground or excited energy eigenstates, we also considered injection of atoms in superposition states produced by $\pi/2$ or $3\pi/2$ coherent pulses. We illustrated the close connection between single-mode and multimode instability, and used the method of Carmichael [17] to calculate the boundaries of the unstable regions in the $(\tau/\tau_r) - x$ plane. We found that, unlike the stationary-atom or single-mode mesomaser case, instability due to the imaginary part of the intracavity field plays a significant role in the multimode analysis. In fact, this is especially true for superposition-state injection, with global instability of a large range of the state equation being achiev-

able using $\pi/2$-pulse preparation. We believe that this is the first observation of such an instability in an optically bistable system using a medium of resonant, homogeneously-broadened atoms.

A physical system in which these effects could be observed consists of a dye-laser (or diode-laser) driven ring cavity with a round-trip path of 50–100 cm, crossed by a fast beam of alkali atoms (atoms ionized, accelerated through 5–10 kV, and neutralized) [18]. Such a beam would be very nearly monoenergetic. Alternatively, one could use a much longer (tens of meters) far-infrared or microwave cavity and a velocity-selected beam of Rydberg atoms. The atomic beam density required is that to reach $C = 5$; for $\tau/\tau_{sp} = 0.1$, an acceptably small value [1], this means the same density as required to achieve $C_{st} = 200$, which is not difficult in a good cavity. The cavity length must be such that the round-trip time is of the same order as the atomic transit time. The fast-atomic-beam system is especially attractive in that it allows for control of the transit time as well as the injected atomic state.

One complication present in most physical systems is that the resonator mode would have a Gaussian profile. This is no problem if the atomic beam has a height small compared to the transverse dimension of the Gaussian profile, so that all atoms can pass through the peak and experience the same effective pulse. If this is not possible, and the height of the atomic beam is much larger than the Gaussian mode waist, the multistable regions would only be reduced in size, not eliminated [1]. However, the effect of the Gaussian mode on the instabilities is still an interesting question open for further investigation. It is known that the multimode instability disappears in a homogenously-broadened resonant system in a Gaussian mode [14], but the evolution of the atomic state in transit suggests that our system might not be similarly restricted. Further investigation is warranted, also, into the dynamics of the transmission of the transit-multistable ring cavity, especially with superposition-state injection. Even more richness in the nonlinear dynamics might be expected here than was observed in the case of excited-state injection [6].

Acknowledgements

The authors gratefully acknowledge valuable discussions with Professor Donna K. Bandy.

References

[1] A.T. Rosenberger, J.-M. Kim, Opt. Commun. 101 (1993) 403.
[2] J.-M. Kim, A.T. Rosenberger, Opt. Commun. 115 (1995) 401.
[3] F. Casagrande, L.A. Lugiato, W. Lange, H. Walther, Phys. Rev. A 48 (1993) 790.
[4] C. Balconi, F. Casagrande, L.A. Lugiato, W. Lange, H. Walther, Opt. Commun. 114 (1995) 425.
[5] C. Balconi, F. Casagrande, A. Mondini, W. Lange, Phys. Rev. A 54 (1996) 898.
[6] M. Benassi, F. Casagrande, W. Lange, Quantum Semiclass. Opt. 9 (1997) 879.
[7] A.N. Oraevsky, T.V. Sarkisyan, D.J. Jones, D.K. Bandy, Kvantovaya Elektron. 19 (1992) 234, Sov. J. Quantum Electron. 22 (1992) 213.
[8] D.K. Bandy, J.D. Graham, D.J. Jones, A.N. Oraevsky, T.V. Sarkisyan, Phys. Rev. A 50 (1994) 685.
[9] D.K. Bandy, J.D. Graham, D.J. Jones, A.N. Oraevsky, T.V. Sarkisyan, Kvantovaya Elektron. 21 (1994) 615, Quantum Electron. 24 (1994) 563.
[10] J. Krause, M.O. Scully, H. Walther, Phys. Rev. A 34 (1986) 2032.
[11] R.R. McGowan, W.C. Schieve, Phys. Rev. A 56 (1997) 2373.
[12] L. Zeng, Z. Liu, Y. Lin, S. Zhu, Phys. Lett. A 246 (1998) 43.
[13] R. Bonifacio, L.A. Lugiato, Lett. Nuovo Cimento 21 (1978) 510.
[14] L.A. Lugiato, M. Milani, Z. Phys. B 50 (1983) 171.
[15] L.A. Lugiato, L.M. Narducci, Phys. Rev. A 32 (1985) 1576.
[16] B. Ségard, B. Macke, L.A. Lugiato, F. Prati, M. Brambilla, Phys. Rev. A 39 (1989) 703.
[17] H.J. Carmichael, Phys. Rev. Lett. 52 (1984) 1292.
[18] H. Pauly, High-energy beam sources, in: G. Scoles (Ed.), Atomic and Molecular Beam Methods, Vol. 1, Oxford University Press, Oxford, 1988, pp. 124–152.